Improving quark flavor separation with forward W and Z production at LHCb

Juan Rojo[*][†]

*Department of Physics and Astronomy, VU University, De Boelelaan 1081, 1081 HV Amsterdam,
and Nikhef Theory Group, Science Park 105, 1098 XG Amsterdam, The Netherlands.*
*E-mail:* j.rojo@vu.nl

We quantify the constraints on the flavour separation between the quarks and antiquarks in the proton provided by the recent forward weak gauge boson production data from the LHCb experiment at $\sqrt{s} = 7$ and 8 TeV. Performed in the framework of the NNPDF3.1 global analysis, this study highlights the key role that the LHCb W and Z data have in achieving a robust quark flavor separation in the large-x region, including the strange and charm quarks. We demonstrate how the LHCb measurements lead to improved determinations of the the up and down quark PDFs in the region $x \gtrsim 0.1$, with an uncertainty reduction that can be as large as a factor 2. We also show how the LHCb forward measurements severely restrict the size of the fitted charm PDF at large x, imposing stringent constraints on non-perturbative models for the charm content of the nucleon.

XXV International Workshop on Deep-Inelastic Scattering and Related Subjects
3-7 April 2017
University of Birmingham, UK

---

[*]Speaker.

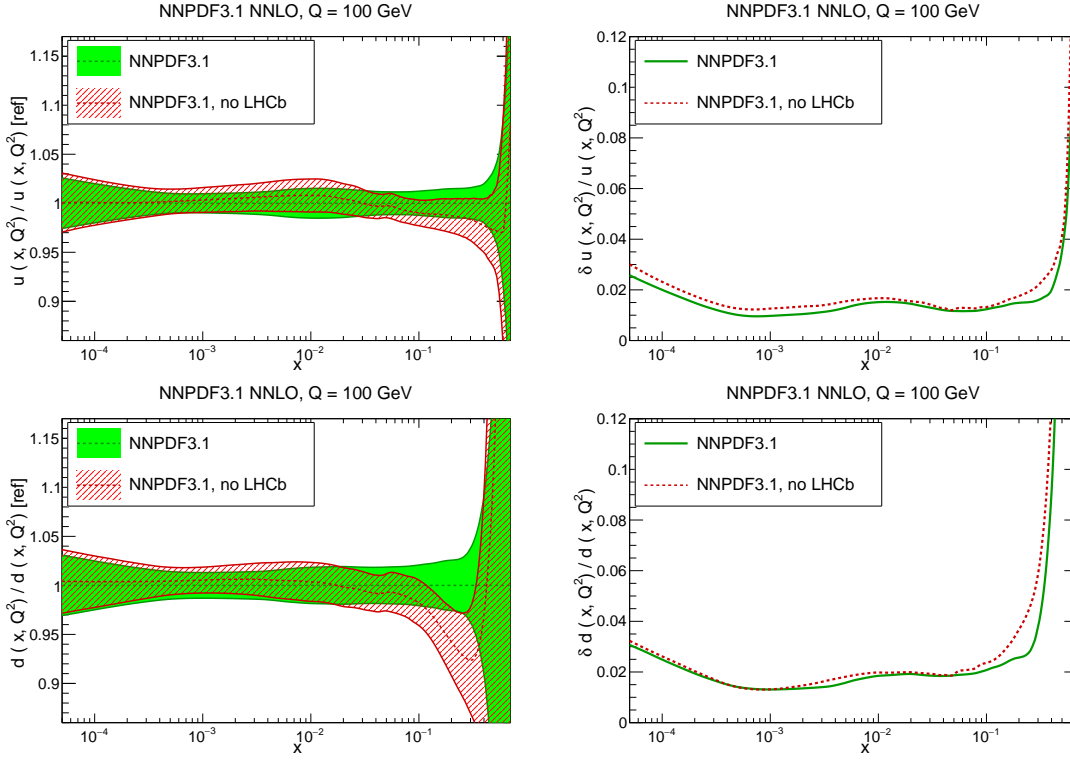[†]On behalf of the NNPDF Collaboration.
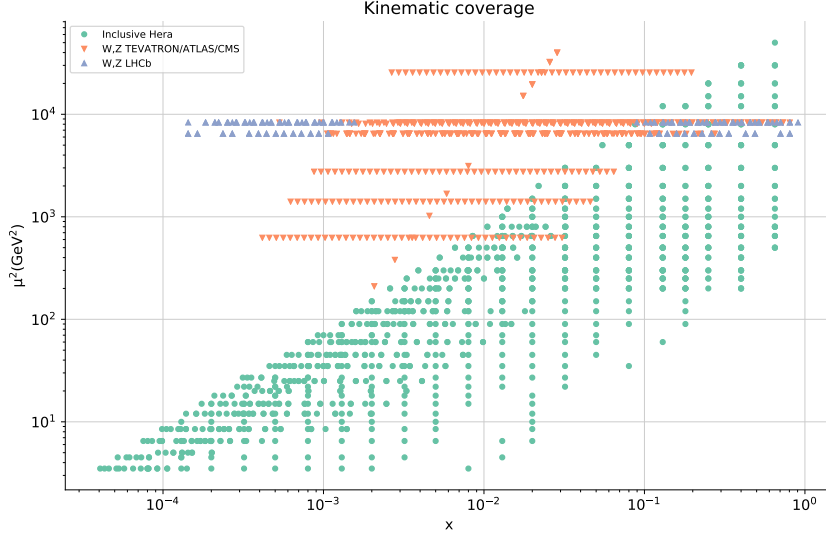
Figure 1: The coverage in the (x, Q^2) plane of the W, Z production data from LHCb, compared with that of W, Z production at ATLAS, CMS and the Tevatron and with that of the HERA structure functions.

The recent NNPDF3.1 global analysis [1] is the latest release from the NNPDF collaboration. It is based on the NNPDF3.0 framework [2] with two main improvements. On the one hand, a large number of new precision collider measurements have been added, including some that for the first time are included in a global fit such as the Z transverse momentum [3] and the differential distributions in top-quark pair production [4]. On the other hand, the charm PDF is now treated on an equal footing as compared of the light quark PDFs [5], that is, in NNPDF3.1 $c(x, Q_0)$ is parametrized with an artificial neural network and then fitted to the data. This improved treatment of the charm PDF has several benefits, among which that of reducing the dependence of high-scale observables to the value of the charm quark mass m_c.

Concerning the new experimental data, a wealth of recent electroweak gauge boson production measurements has been included in NNPDF3.1. These datasets provide useful information on the separation between different quark flavours, including strange and charm, as well as between quarks and antiquarks. In this respect, the forward weak boson production measurements presented by the LHCb collaboration are particularly interesting to access the large-x region [6], where PDF uncertainties are the largest. NNPDF3.1 includes the complete LHCb $\sqrt{s} = 7$ and 8 TeV measurements of inclusive W and Z production in the forward region in the muon channel [7, 8], which supersede all previous measurements in the same final state. These new measurements complement earlier LHCb data already included in NNPDF3.0 [9, 10]. In this contribution, we explore the impact of the LHCb data on the NNPDF3.1 analysis and show how sizable constraints are derived at large-x for all the light quark PDFs and for the charm PDF. In turn, this leads to reduced theoretical uncertainties for the production of new massive BSM resonances, which are dominated currently by the large-x PDF uncertainties [11].

Let us also mention that another set of recent LHCb measurements that have revealed an unexpected usefulness for PDF studies is forward D meson production [12, 13]. As demonstrated in [14], the combination of LHCb charm production data at $\sqrt{s} = 5, 7$ and 13 TeV leads to a

Figure 2: The up quark (upper plots) and down quark (lower plots) PDFs at $Q = 100$ GeV, comparing the results of the NNPDF3.1 baseline with those of the corresponding fit without LHCb data. We show the PDF ratios normalized to the central value of NNPDF3.1 (left) and the relative PDF uncertainties (right plots).

reduction of the PDF uncertainties on the gluon at $x \simeq 10^{-6}$ by up to an order of magnitude.

Forward weak boson production at LHCb. In Fig. 1 we show the kinematical coverage in the (x, Q^2) plane of the W and Z production data from LHCb included in NNPDF3.1, compared with the corresponding coverage of W, Z production at ATLAS, CMS and the Tevatron, as well as with that of the HERA inclusive structure function data. For the Drell-Yan data, the values of (x, Q^2) for each data bin are approximated assuming leading order kinematics, namely $x_{1,2} = (M/\sqrt{s})e^{\pm y}$, with M and y the invariant mass and the lepton rapidity of each bin. We observe that the LHCb data spans a wider and complementary range in x as compared from the ATLAS and CMS measurements, and in particular ensure an improved coverage of the large-x region.

In order to illustrate the impact of the LHCb data, in Fig. 2 we show the up quark and down quark PDFs at $Q = 100$ GeV, comparing the results of the NNPDF3.1 NNLO fit with those of the same fit without any LHCb data. We show the PDF ratios normalized to the central value of NNPDF3.1 and the relative PDF uncertainties. From this comparison, we see that the LHCb data has a significant impact in NNPDF3.1, both in terms of shifting the central value of the large-x quarks, where the LHCb data prefer larger values, and in terms of reducing the PDF uncertainties. In the case of $xd(x, Q)$, the LHCb data reduce the PDF uncertainties by almost a factor 2 for $x \simeq 0.3$.

Next, in Fig. 3 we show the quark-quark PDF luminosity $\mathscr{L}_{qq}$ and its relative uncertainty for the NNPDF3.1 fits with and without the LHCb data. We find that the LHCb data prefers harder $\mathscr{L}_{qq}$
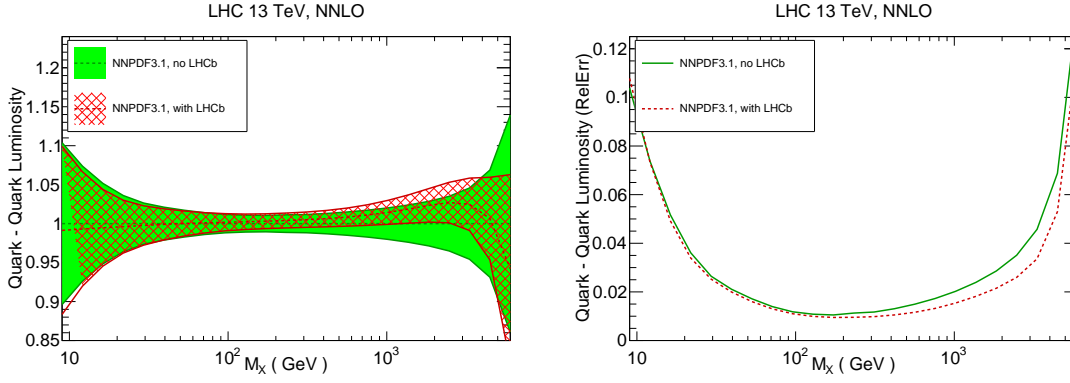
Figure 3: The quark-quark PDF luminosity (left plot) and its relative uncertainty (right plot) comparing the NNPDF3.1 fits with and without the LHCb data included.

values in the TeV region, and also that it leads to an important reduction of the PDF uncertainties in the same region.

In order to quantify the improvement in the description of the LHCb data achieved in the NNPDF3.1 analysis, in Table 1 we show the $\chi^2/N_{\rm dat}$ values for the individual LHCb datasets included in NNPDF3.1 (as well as their total) for three NNLO different fits: NNPDF3.1, NNPDF3.1 no LHCb, and NNPDF3.0. The numbers in brackets indicate those datasets not included in the corresponding fits. We see that NNPDF3.1 achieves a good description of the four LHCb datasets, markedly improving on the NNPDF3.0 predictions for the new 7 and 8 TeV measurements. We have also verified that the use of NNLO theory is crucial to achieve satisfactory $\chi^2/N_{\rm dat}$ values.

| Dataset	NNPDF3.1	NNPDF3.1 no LHCb	NNPDF3.0
LHCb Z 940 pb	1.4	[1.7]	1.3
LHCb $Z \to ee$ 2 fb	1.1	[1.0]	1.2
LHCb $W, Z \to \mu$ 7 TeV	1.7	[4.4]	[2.6]
LHCb $W, Z \to \mu$ 8 TeV	1.4	[3.4]	[2.4]
LHCb total	**1.5**	**[3.1]**	**2.1**

Table 1: The $\chi^2/N_{\rm dat}$ for the individual LHCb datasets included in NNPDF3.1 (as well as their total) for three different NNLO fits. The numbers in brackets indicate datasets not included in the corresponding fit.

To further illustrate the improved agreement between theory and data, in Fig. 4 we show the comparison between the NNPDF3.1 and NNPDF3.0 NNLO predictions and the LHCb data on the lepton rapidity distribution in W^+ production at 8 TeV in the muon final state, normalized to the central value of the experimental data. We observe that not only the agreement is improved at the level of central values, specially in the forward region, but also that the PDF uncertainties for individual bins are reduced by up to a factor two in NNPDF3.1. In the same figure we also show the corresponding comparison for the Z rapidity distributuon, now in terms of the absolute cross-section. Also in this case we observe how the central values of the NNPDF3.1 prediction move closer to the data as compared to the NNPDF3.0 ones. It is also worth emphasizing that for all the LHCb datasets the agreement between NNLO theory and data is markedly better than at NLO.

Constraining the charm content of the proton. In the NNPDF3.1 global analysis, the charm
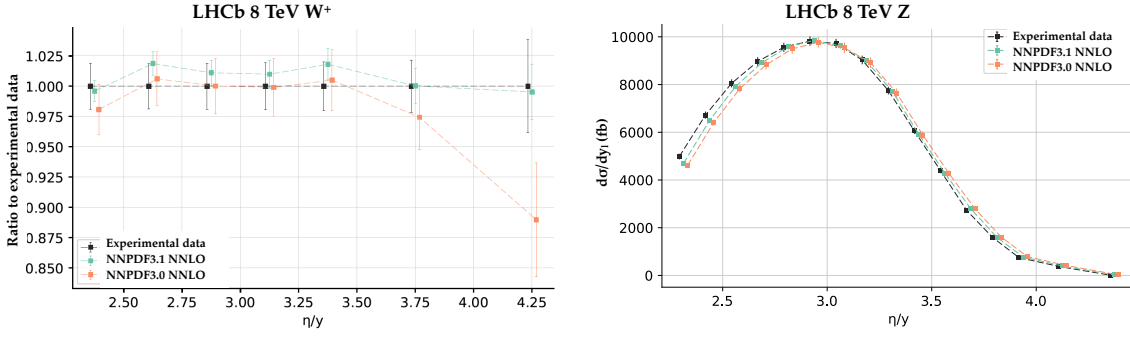
Figure 4: Left plot: comparison between the NNPDF3.1 and NNPDF3.0 NNLO predictions and the LHCb data on W^+ production at 8 TeV in the muon final state, normalized to the central value of the experimental data. Right plot: same comparison for the Z rapidity distributuon, now in terms of the absolute cross-section.
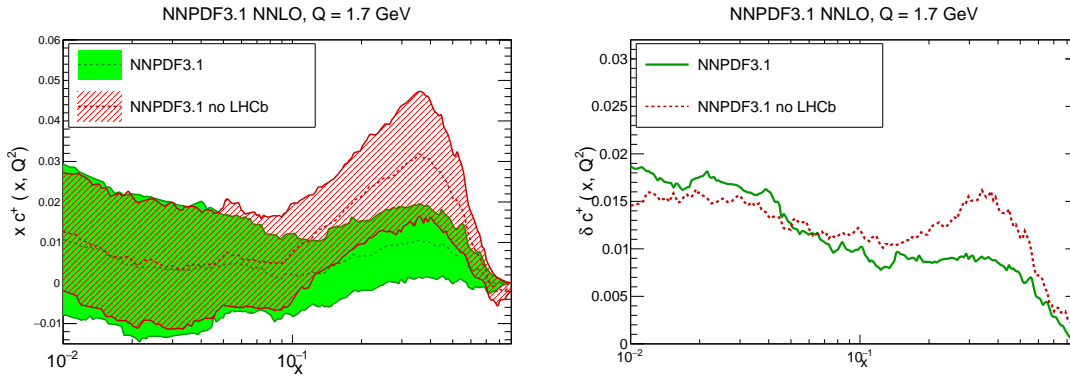
Figure 5: Left plot: the charm PDF $xc^+(x,Q^2)$ at $Q = 1.7$ GeV, comparing the results of the NNPDF3.1 fit with those of the same fit excluding the LHCb data. Right plot: the decrease in the absolute PDF uncertainties of the charm PDF at the same scale $Q = 1.7$ GeV once the LHCb data is included.

PDF is parametrized at the input scale $Q_0 \gtrsim \mu_c$, with $\mu_c = m_c$ being the charm threshold, and then determined from experimental data in the same way as the light quark PDFs. It can be shown that the forward W, Z production data from LHCb provide, in addition to constrains on the light quark PDFs, also useful information on the charm content of the proton. This sensitivity can be understood from the fact that forward gauge boson production depends on charm PDF via partonic subprocesses such as $\bar{s}c \to W^+$ and $s\bar{c} \to W^-$.

In Fig. 5 we show the charm PDF $xc^+(x,Q^2)$ at $Q = 1.7$ GeV and its absolute uncertainty δc^+ for the fits with and without LHCb data. We observe how the LHCb measurements lead to a suppressed xc^+ at large-x, as well as to a reduction of the associated PDF uncertainties. These results indicate that stringent constraints on models of the non-perturbative charm content of the proton can be provided by the LHCb W, Z data.

The impact of the LHCb data on the charm PDF can also be gauged by computing $\langle xc \rangle$, the average momentum fraction carried by charm quarks in the proton, for the NNPDF3.1 fits with and without the LHCb data. When LHCb data is excluded we find that, for $Q = Q_0 = 1.65$ GeV, $\langle xc \rangle_{\mathrm{noLHCb}} = 0.012 \pm 0.006$, while in the baseline NNPDF3.1 fit we have instead $\langle xc \rangle_{3.1} = 0.004 \pm 0.004$. This is a consequence that, as shown in Fig. 5, both the central value is reduced

and the PDF error decreases. It is also interesting to note that, after the addition of the EMC charm data (which is not part of the NNPDF3.1 dataset), one finds $\langle xc \rangle_{3.1+EMC} = 0.005 \pm 0.001$, a central value consistent with the one preferred by LHCb. These results confirm the importance of the forward W, Z LHCb data for our understanding of the charm content of the nucleon.

References

[1] **NNPDF** Collaboration, R. D. Ball et al., *Parton distributions from high-precision collider data*, in preparation.

[2] **NNPDF** Collaboration, R. D. Ball et al., *Parton distributions for the LHC Run II*, *JHEP* **04** (2015) 040, [arXiv:1410.8849].

[3] R. Boughezal, A. Guffanti, F. Petriello, and M. Ubiali, *The impact of the LHC Z-boson transverse momentum data on PDF determinations*, arXiv:1705.00343.

[4] M. Czakon, N. P. Hartland, A. Mitov, E. R. Nocera, and J. Rojo, *Pinning down the large-x gluon with NNLO top-quark pair differential distributions*, *JHEP* **04** (2017) 044, [arXiv:1611.08609].

[5] **NNPDF** Collaboration, R. D. Ball, V. Bertone, M. Bonvini, S. Carrazza, S. Forte, A. Guffanti, N. P. Hartland, J. Rojo, and L. Rottoli, *A Determination of the Charm Content of the Proton*, *Eur. Phys. J.* **C76** (2016), no. 11 647, [arXiv:1605.06515].

[6] R. S. Thorne, A. D. Martin, W. J. Stirling, and G. Watt, *Parton Distributions and QCD at LHCb*, in *Proceedings, 16th International Workshop on Deep Inelastic Scattering and Related Subjects (DIS 2008): London, UK, April 7-11, 2008*, p. 30, 2008. arXiv:0808.1847.

[7] **LHCb** Collaboration, R. Aaij et al., *Measurement of the forward Z boson production cross-section in pp collisions at $\sqrt{s} = 7$ TeV*, *JHEP* **08** (2015) 039, [arXiv:1505.07024].

[8] **LHCb** Collaboration, R. Aaij et al., *Measurement of forward W and Z boson production in pp collisions at $\sqrt{s} = 8$ TeV*, *JHEP* **01** (2016) 155, [arXiv:1511.08039].

[9] **LHCb** Collaboration, R. Aaij et al., *Inclusive W and Z production in the forward region at $\sqrt{s} = 7$ TeV*, *JHEP* **1206** (2012) 058, [arXiv:1204.1620].

[10] **LHCb** Collaboration, R. Aaij et al., *Measurement of the cross-section for $Z \to e^+e^-$ production in pp collisions at $\sqrt{s} = 7$ TeV*, *JHEP* **1302** (2013) 106, [arXiv:1212.4620].

[11] W. Beenakker, C. Borschensky, M. Kramer, A. Kulesza, E. Laenen, S. Marzani, and J. Rojo, *NLO+NLL squark and gluino production cross-sections with threshold-improved parton distributions*, *Eur. Phys. J.* **C76** (2016), no. 2 53, [arXiv:1510.00375].

[12] **PROSA** Collaboration, O. Zenaiev et al., *Impact of heavy-flavour production cross sections measured by the LHCb experiment on parton distribution functions at low x*, *Eur. Phys. J.* **C75** (2015), no. 8 396, [arXiv:1503.04581].

[13] R. Gauld, J. Rojo, L. Rottoli, and J. Talbert, *Charm production in the forward region: constraints on the small-x gluon and backgrounds for neutrino astronomy*, *JHEP* **11** (2015) 009, [arXiv:1506.08025].

[14] R. Gauld and J. Rojo, *Precision determination of the small-x gluon from charm production at LHCb*, *Phys. Rev. Lett.* **118** (2017), no. 7 072001, [arXiv:1610.09373].